Atmospheric Research 222 (2019) 163–171

Contents lists available at ScienceDirect

Atmospheric Research

journal homepage: www.elsevier.com/locate/atmosres

Modeling lightning density using cloud top parameters

Athanasios Karagiannidis[a,*], Konstantinos Lagouvardos[a], Spyridon Lykoudis[b,1], Vassiliki Kotroni[a], Theodore Giannaros[a], Hans-Dieter Betz[c]

[a] Institute of Environmental Research and Sustainable Development, National Observatory of Athens, Athens, Greece
[b] 66, Akrita str., GR-24132 Kalamata, Greece
[c] Ludwig-Maximilians-University Munich and Nowcast GmbH, Munich, Germany

ARTICLE INFO

Keywords:
Lightning density
NWC SAF
LINET
Convective cloud tops
Europe

ABSTRACT

The Price-Rind 92 parameterization (Price and Rind, 1992) that utilizes cloud top height as predictor for the estimation of lightning density is widely used by modelers in an attempt to forecast electrical activity in thunderstorms. In the present paper new parameterizations for the estimation of lightning density of convective clouds are formulated. LINET lightning data, NWC SAF (Satellite Application Facility on support to Nowcasting and Very Short-Range Forecasting) products and ERA-Interim (ECMWF-Re Analysis) data, covering the summer of 2016 over continental Europe, are used. The proposed models estimate the lightning density of convective clouds, using cloud top height, cloud top pressure and cold cloud depth as predictors. Model efficiency statistics calculated over an independent dataset, suggest that the proposed models can be considered successful over the specific area (continental Europe) and period (summer). The new cloud top height model differs from the PR92 and other parameterizations, which is not an unexpected result, since every model has its own characteristics, strengths and weaknesses. The new parameterizations could be utilized in numerical model simulations to produce quantitative estimations of the amount of strokes over convective areas.

1. Introduction

Lightning is a spectacular but potentially dangerous phenomenon. Wildfires (Flannigan and Wotton, 1991; Rorig and Ferguson, 1999; Liu et al., 2010; Peterson et al., 2010), industrial accidents (Chang and Lin, 2006; Renni et al., 2010; Krausmann et al., 2011), aviation accidents (Cherington and Mathys, 1995) and human fatalities in general (Coates et al., 1993; Ashley and Gilson, 2009; Elsom, 2001; Cardoso et al., 2014; Papagiannaki et al., 2013) are some of the possible outcomes of the atmospheric electrical phenomena. Such a dangerous but at the same time interesting phenomenon merits and of course receives tremendous attention by weather scientists and researchers. Forecasting and nowcasting are included in the most important fields in the research on lightning.

Barthe et al. (2010) used the Weather Research and Forecasting Model (WRF) to simulate two thunderstorms over the US, and investigated the effectiveness of a set of parameters as a proxy for lightning flash rate prediction. They found that the most reliable parameters were the precipitation ice mass and maximum vertical velocity. In an effort to nowcast lightning, Kohn et al. (2011) used the ZEUS VLF lightning detection network and the Warning Decision Support System-Integrated Information (WDSS-II) software. They simulated lightning form thousands of thunderstorms up to 2 h ahead and showed that their algorithm was very successful in locating lightning clusters. Wong et al. (2013) implemented the Price-Rind (Price and Rind, 1992) Lightning Parameterization Scheme (hereafter PR92) in the WRF model and evaluated its performance for simulating lightning activity over the United States. It was shown that although the integrated flash count agrees with observations when model biases in convection are taken into account, significant problems were identified on the simulation of the frequency distribution. Zepka et al. (2014) attempted to predict lightning over Brazil. They developed the Potential Lightning Region (PLR) method which combines various WRF variables and estimates the probability of the occurrence of lightning over a region. Their method performed better when lightning data was also utilized as input. Giannaros et al. (2015) attempted to predict lightning activity during ten events over Greece, using the WRF model. They found that the overestimation of the activity could be significantly reduced after implementing microphysics and thermodynamics masks, with the better results occurring with the combined use of the total ice content, the

* Corresponding author.
E-mail address: thankar@live.com (A. Karagiannidis).
[1] Independent Scholar.

https://doi.org/10.1016/j.atmosres.2019.02.013
Received 24 December 2018; Accepted 20 February 2019
Available online 21 February 2019
0169-8095/

maximum vertical velocity and the convective potential available energy (CAPE). In continuation to the aforementioned work, Giannaros et al. (2016) has shown, based on the verification of 1-year of lightning forecasts, that the application of masking filtering was necessary for the improvement of lightning forecasts for all three convective parameterization schemes employed. Karagiannidis et al. (2016) employed MSG IR imagery and real-time data from the ZEUS VLF lightning detection network in order to nowcast lightning manifestation over Greece over a period of 1 h. Their validation showed an acceptable degree of success and their tool was considered fit for operational use. Pytharoulis et al. (2016) studied a heavy precipitation event in northern Greece, using the Lightning Potential Index proposed by Yair et al. (2010), and obtained a lot of useful conclusions regarding the efficiency of simulations on intense precipitation events, influenced by both synoptic forcing and topographic effects. Gijben et al. (2017) used lightning data from the Southern Africa Lightning Detection Network along with parameters computed by the Unified Model and developed a Lightning Threat Index (LTI) for the warm part of the year. As they showed LTI is sensitive and specific enough, although it over-forecasts lightning during spring.

Part of the algorithms and methods utilized to forecast lightning by numerical models are based on the PR92, proposed in Price and Rind (1992). The authors formulated two different parameterizations, one for continental and one for maritime thunderstorms. The continental formula suggests that the flash rate frequency (in flashes per minute) is almost proportional to the fifth power of the storm height ($F_c = 3.44 \cdot 10^{-5} \cdot H^{4.9}$ where F_c is the flash rate and H the thunderstorm height in km). The maritime formula suggests that the flash rate is almost proportional to the second power of the storm height ($F_c = 6.4 \cdot 10^{-4} \cdot H^{1.73}$). In the following years, several researchers attempted to utilize or reassess the PR92 parameterization. For example Michalon et al. (1999), following the suggestions of Molinié and Pontikis (1995, 1996), introduced a new parameterization where the cloud droplet concentration is included, unifying thus the continental and maritime formulas. They argued that the introduction of the cloud droplet concentration improved the estimation efficiency of the flash rate. Ushio et al. (2001) addressed the relationship between storm height and flash rate over several regions, using Tropical Rainfall Measuring Mission (TRMM) satellite data. They showed that this relationship is nonlinear and presents large variance, and also that the flash rate increases with storm height, but there are cases of tall thunderstorms with rather low flash rates. Moreover, discrepancies between seasons were identified. Overall they concluded that although the fifth power scaling law of PR92 was not inconsistent with their data, it wasn't always the best fit. Yoshida et al. (2009) examined the relationship between the number of flashes per second per convective cloud and the cold-cloud depth, the latter being defined as the height of the cloud above melting point. They concluded that the fifth power law is adequate to describe this relationship, both for continental and maritime storms. Boccippio (2002), although placed significant questions about the consistency of the underlying theory of the PR92 maritime parameterization, accepted that a purely empirical fine-tuning of the relationship may lead to useful approximations of the lightning activity based on geometrical features of the storms. According to Barthe et al. (2010), who simulated two storms over the US using the WRF model, the cloud top height can be used to estimate the flash rate trend and value, only for the airmass thunderstorm case. Finally, Giannaros et al. (2015) who assessed the efficiency of a lightning activity algorithm based on the PR92 parameterization in WRF model, showed that after implementing a mask based on total ice content, maximum vertical velocity and CAPE, the PR92 parameterization presented very good results on estimating the severity of the lightning activity.

In the present paper we attempt to formulate simple models to estimate lightning density (LD) associated with convective clouds. To do that we utilize the number of total lightning strokes, in relation to the highest altitude of the surrounding cloud top pixels. We use the term "altitude" in a general sense, to include the Cloud Top Height (CTH) in kilometers, and the Cloud Top Pressure (CTP) in hPa. Those two measures of cloud top "altitude" are computed using EUMETSAT's (European Organisation for the Exploitation of Meteorological Satellites) NWC SAF v2013 CTTH (Cloud Top Temperature and Height) product, for the Meteosat satellites. The source code of the NWC SAF package is freely available to users in possession of a license agreement with EUMETSAT. The National Observatory of Athens (NOA) has installed and operates the package on a Unix platform since the summer of 2015. More about NWC SAF can be found in (http://www.nwcsaf.org/, last accessed on 12/11/2018).

The 2013 version of NWC SAF, which is used in the present analysis, in its general configuration requires input of real time satellite data in High Rate Information Transmission (HRIT) format. For many of its products, numerical weather prediction (NWP) fields are also mandatory. We use the Weather Research and Forecasting model (WRF), version 3.6.1 (Skamarock et al., 2008) to produce the necessary NWP inputs.

In section 2 the software and models that are used are briefly presented. Section 3 includes the description of the data and section 4 depicts the methodologies used in the analysis. The results are presented and discussed in section 5, while section 6 summarizes and discusses the main conclusions of the analysis.

2. Algorithms and models

The data analyzed in our work have been mainly produced by the NWC SAF v2013 for Meteosat Satellites, and by the WRF version 3.6.1 model, which are described in this section.

2.1. The NWC SAF package

The primary goal of the NWC SAF package is the generation of meteorological products that could be used for the support of nowcasting and very short range forecasting. Each of the products is generated by a Product Generator Element (PGE). The package includes a Task Manager (TM) which is able to execute all necessary tasks for the generation of NWC SAF products in real-time operational mode with minimum user interference. As stated earlier, NWC SAF uses satellite images from the Meteosat Satellites and other required data (e.g. NWP forecasts) as inputs. However, several PGEs require other PGEs outputs to be executed correctly. This task is appointed to the TM that manages, among others, the in-sequence execution of various modules. Fig. 1 illustrates the basic NWC SAF architecture in a very simple way. For more information about NWC SAF the reader is referred to NWC SAF website http://www.nwcsaf.org and the related documentation.

In our analysis we use the "Cloud Type" (CT – PGE02), the "Cloud Top Temperature and Height" (CTTH – PGE03), and the "Convective

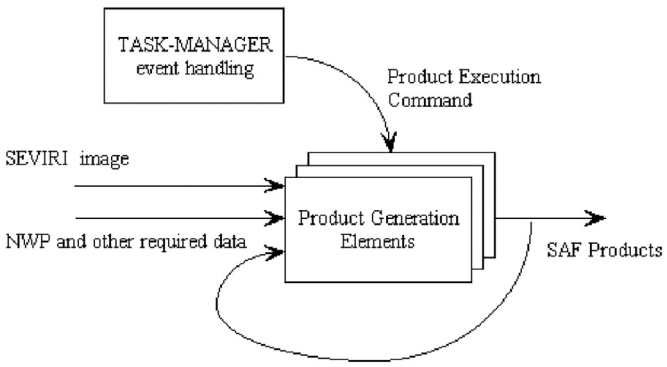

Fig. 1. Simplified NWC SAF/MSG design (image from EUMESAT Nowcasting Consortium, 2013).

Table 1
Average cloud top pressure ranges for the altitude-defined opaque cloud types.

Very low opaque clouds	Barometric pressure higher than 800 hPa
Low opaque clouds	Barometric pressure between 650 and 800 hPa
Medium opaque clouds	Barometric pressure between 450 and 650 hPa
High opaque cloud	Barometric pressure between 300 and 450 hPa
Very high opaque clouds	Barometric pressure lower than 300 hPa

Rainfall Rate" (CRR – PGE05) product.

2.1.1. The Cloud Type (CT) product

The CT product is required as input by the CTTH algorithm and therefore the CT computation takes precedence over the implementation of the CTTH algorithm. It classifies all cloudy pixels in the following major categories: fractional clouds, semitransparent clouds, opaque clouds, very low clouds, low clouds, medium clouds, high clouds and very high clouds. The average cloud top pressure levels thresholds for the altitude-defined opaque cloud types are presented in Table 1.

The channels of the Spinning Enhanced Visible and Infrared Imager (SEVIRI) radiometer onboard the MSG satellites that are necessary for the CT algorithm execution are presented in Table 2. They are categorized as mandatory or optional. As expected, when a mandatory channel is missing, the product is not generated.

Besides the SEVIRI input, certain NWP parameters are also required as input: (i) surface temperature, (ii) air temperature at 950 hPa (or 925 hPa), 850 hPa, 700 hPa, 500 hPa and at the tropopause level, (iii) total water vapour content of the atmosphere, (iv) altitude from the NWP model grid (alternatively surface geopotential from the NWP model grid). In the case that these parameters are not available, the NWC SAF package replaces them with ancillary datasets and computing methods.

A series of ancillary datasets, remapped in the MSG native grid is also required and included in the NWC SAF package: (i) land/sea atlas, (ii) elevation atlas, (iii) monthly minimum SST climatology, (iv) monthly mean 0.6 μm atmospheric-corrected reflectance climatology over land, (v) monthly 0.6 μm and 1.6 μm white-sky surface albedo climatology over land, (vi) monthly integrated atmospheric water vapour content climatology and (vii) monthly climatology of mean air temperature at 1000 hPa, 850 hPa, 700 hPa, 500 hPa.

Finally, two static files are also included. The first contains satellite-dependent values and look-up tables for thresholds required for the characterization of each pixel. The second contains offline simulations of 0.6 μm and 1.6 μm reflectances performed for a set of four water and four ice clouds using a radiative transfer model called RTMOM (Radiative Transfer based on Matrix Operator Method).

2.1.2. The CTTH product

Table 3 presents the channels of the SEVIRI radiometer that are required for the computation of the CTTH product. In the case that the T10.8 μm brightness temperature is missing, the product is not computed. On the other hand, when the T10.8 μm brightness temperature is available, but some of the mandatory channels are missing, the cloud top temperature is computed, but the cloud top pressure and height is not.

Regarding the NWP forecast input, CTTH requires: (i) surface temperature, (ii) surface pressure, (iii) air temperature and relative humidity (or dew point temperature) at 2 m, (iv) air temperature and relative humidity on vertical pressure levels, and (v) altitude (or surface geopotential) on the model grid. All these parameters are remapped to the MSG native grid by the NWC SAF package.

Table 3
SEVIRI brightness temperatures (T) and reflectances (R) needed at full IR spatial resolution for the computation of the CTTH product (from Derrien and Le Gléau, 2013a).

Rad6.2 μm	Rad7.3 μm	Rad13.4 μm	Rad10.8 μm	T10.8 μm	T12.0 μm
At least one of these channels is mandatory, the two others are then optional			Mandatory	Mandatory	Optional

Mandatory ancillary datasets consist of: (i) land/sea atlas, (ii) elevation atlas, (iii) monthly minimum SST climatology, (iv) monthly mean 0.6 μm atmospheric-corrected reflectance climatology (land). These datasets are included in the software package in the MSG native grid.

A file containing satellite-dependent coefficients values and a look-up table for climatologic atmospheric absorption corrections that are required by the CTTH product, is also included.

Finally, the RTTOV-9 radiative transfer model (developed by NWP SAF; more can be found in https://www.nwpsaf.eu/site/, last accessed on 12/11/2018) is also applied. It simulates the 6.2 μm, 7.3 μm, 13.4 μm, 10.8 μm, and 12.0 μm cloud free and overcast reflectances and brightness temperatures using NWP temperature and humidity vertical profiles. The vertical profiles used are temporally interpolated to the exact slot time using the two nearest in time NWP input fields. The required coefficients are given in a file that is included in the downloaded software package.

Both CT and CTTH outputs are offered in HDF format. The main fields are the cloud type (CT product), the cloud top temperature, the cloud top pressure, and the cloud top height (CTTH product), along with a series of quality parameters. More about the algorithm theoretical basis, the user's manual and the validation of the CT and CTTH product can be found in Derrien and Le Gléau (2013a, 2013b, 2013c).

2.1.3. The CRR product

The mandatory SEVIRI channels for the computation of the CRR product are shown in Table 4. TPrev10.8 μm is defined as the difference of the 10.8 μm brightness temperature between the present time slot and the previous one. It is a measure of the cloud growth rate and it is used to compute the Cloud Growth Rate Correction Factor. When it is not available, the Cloud Growth Rate Correction Factor is not computed but a correction factor (named Cloud-top Temperature Gradient Correction Factor) is computed and used as an alternative.

The required NWP fields are: (i) relative humidity at various pressure levels, (ii) dew point temperature at 2 m, (iii) temperature at 2 m, (iv) temperature at various pressure levels, (v) surface pressure, (vi) geopotential at various pressure levels, and (vii) U and V wind components at 850 hPa.

The following static fields, which are included or computed by the software package are also needed: (i) sun angles associated to SEVIRI imagery (ii) saturation vapour table for humidity correction, (iii) saturation vapour polynomial coefficients table for humidity correction, (iv) elevation mask for orographic correction, (v) climatological profile as a backup for Parallax correction in case NWP is not available.

CRR outputs are in HDF format. They include the CRR intensity, which is utilized here, and also a series of quality parameters. More

Table 2
SEVIRI brightness temperatures (T) and reflectances (R) needed at full IR spatial resolution for the computation of the CT product (from Derrien and Le Gléau, 2013a).

R0.6 μm	R1.6 μm	T3.9 μm	T7.3 μm	T8.7 μm	T10.8 μm	T12.0 μm
Mandatory	Optional	Mandatory	Optional	Optional	Mandatory	Mandatory

Table 4
SEVIRI brightness temperatures (T) and reflectances (R) needed at full IR spatial resolution for the computation of the CRR product (from Rodríguez et al., 2013a).

T10.8 μm	TPrev10.8 μm	T6.2 μm	VIS0.6 μm
Mandatory	Optional	Mandatory	Optional

about the algorithm theoretical basis, the user's manual and the validation of the CRR product can be found in Rodríguez et al. (2013a, 2013b, 2013c).

2.2. The WRF model

As stated earlier, the WRF version 3.6.1 numerical model is employed to produce the necessary NWP inputs for the NWC SAF package. The simulations are carried out on two 1-way nested domains with horizontal grid spacing of 24 km covering the European continent. The Dudhia (Dudhia, 1989) and the Rapid Radiative Transfer Model (RTTM), described in Mlawer et al. (1997), schemes are utilized to produce the necessary NWP inputs for shortwave and longwave radiation. Microphysics are handled by the Thompson parameterization (Thompson et al., 2008). The planetary boundary layer is parameterized by the Mellor–Yamada–Janjic (MYJ) parameterization scheme (Janjic, 1994), coupled with the Eta similarity scheme (Janjic, 1996, 2002) for the representation of the surface layer. The Noah land surface model (Tewari et al., 2004), deals with the land surface interactions. Finally, the Kain-Fritsch scheme (Kain, 2004) handles the convection parameterizations.

Initial conditions are extracted by the daily 00:00 UTC 0.5° × 0.5° spatial resolution and 6-h temporal resolution Global Forecast System (GFS) data, which are provided by the National Centre for Environmental Predictions (NCEP). High-resolution (0.083° × 0.083°) sea-surface temperature analyses, provided by NCEP, are also used for the initialization. The model forecasts are initialized daily at 0000 UTC (t + 0) and they extend to t + 84 h, allowing for a 12-h spin-up of the WRF model.

3. Data

Our data are divided in two groups: (i) observational and (ii) simulated data.

3.1. Observational data

The observational data consist of LINET strokes lightning data, namely, latitude and longitude of each stroke. LINET is a ground based, Very Low Frequency / Low Frequency (VLF/LF) lightning detection network with 3D capability. The network is operated by nowcast GmbH, the official provider of lightning data for the German Weather Service, since 2006 when it started with approximately 65 sensors. At the moment (2018) it is comprised of over 150 sensors deployed throughout Europe, and it covers quite densely the European continent (indicative covered region according to Betz et al. (2009b): 10°W-35°E, 30°N-65°N). It can discriminate between cloud-to-ground (CG) flashes and in-cloud flashes (IC), implementing a 3D time-of-arrival (TOA) method, which is quite efficient within the denser regions of the network. Its average detection accuracy is around 150 m. More about the LINET network can be found in Betz et al. (2009a, 2009b).

For the present analysis 3 months of LINET data, specifically from June, July and August of 2016 have been used. During these months, significant atmospheric electrical activity was recorded over the European continent. In order to have high quality data with homogenous and consistent detection efficiency, we constrained the examined area between 10°N-30°N and 45°N-55°N (.

Fig. 2), where the LINET network is known to have its optimum coverage and efficiency. Therefore, all results and conclusions can be regarded as representative of the summertime period over continental mid-latitude regions.

3.2. Simulated data

Two simulated datasets are used in this work. The first consists of archived output near real-time fields of the NWC SAF v2013, specifically the CT, CTTH and CRR products, which were described in Section 2.1. They also cover the June–July–August 2016 period, over the 10°N-30°N / 45°N-55°N region.

The second consists of ERA-Interim reanalysis data, available from the ECMWF Public Datasets web interface (http://apps.ecmwf.int/datasets/, last accessed on 12/11/2018). The spatial resolution is approximately 80 km on 60 vertical levels from the surface up to 0.1 hPa. More about the ERA-Interim datasets can be found in Berrisford et al. (2011) and Dee et al. (2011). In the present work we use the temperature parameter estimated at all the available levels (1000–0.1 hPa), which is available every 6 h (00:00, 06:00, 12:00 and 18:00 UTC).

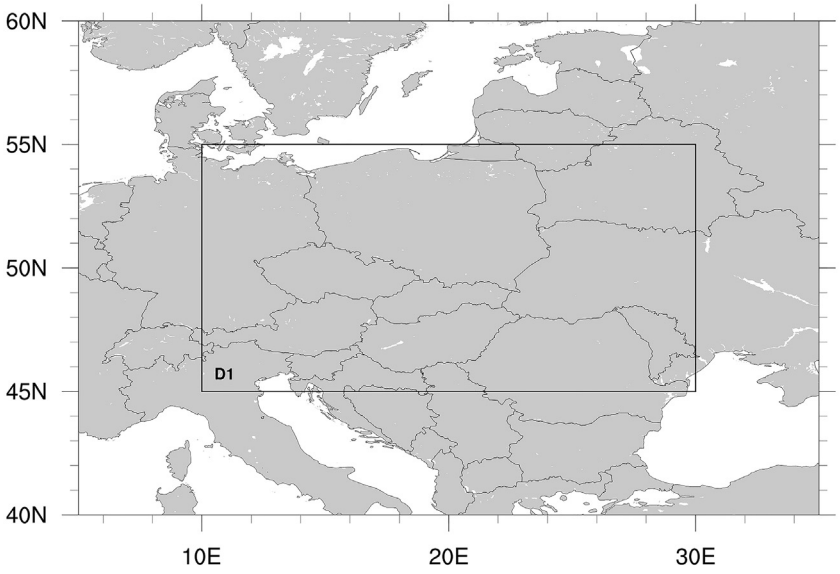

Fig. 2. The analysis domain (D1).

4. Methodology

We examined 3 cloud top related parameters, namely the cloud top height (CTH), the cloud top pressure (CTP), and the cold cloud depth (CCD). The first two are direct outputs of the NWC SAF software and are available every 15 min. Regarding the last one, it was introduced by Yoshida et al. (2009), who computed the parameter by subtracting the height of the freezing level from the cloud top height. The authors estimated the freezing level height by dividing the Sea Surface Temperature (SST) with the moist adiabatic temperature lapse rate ($6\ ^{\circ}K{\cdot}km^{-1}$). In the present work we computed the CCD in pressure units by subtracting the cloud top pressure extracted from the NWC SAF products, from the freezing point level pressure derived from ERA-Interim. The freezing point level was computed using linear interpolation between the two pressure levels that presented the negative and positive temperature values closest to zero. It should be mentioned here that, since the ERA-Interim data are available every six hours (00:00, 06:00, 12:00 and 18:00 UTC), the CCD was also computed for the same hours.

Three preliminary screening procedures were applied to CTH and CTP (and consequently CCD) data before any further analysis, aiming to exclude cloud pixels, which are not related to convection and lightning.

Firstly, the CT of each cloudy pixel, estimated by the CT product of NWC SAF, was checked. All high and very high semi-transparent cloudy pixels were excluded since semi-transparent pixels are not part of opaque cumulonimbus clouds. Fractional pixels were also excluded because their actual nature is ambiguous. Finally all kinds of low and very low clouds are rarely producing lightning, and excluding them is a rather beneficial compromise in terms of computational time.

Secondly, the CRR value of each cloudy pixel was checked. In the case that it was found to be non-available, meaning that no convective rainfall is expected, the pixel was discarded. The possibility to exclude misclassified pixels, should not affect significantly our analysis, since convective pixels with strong convective nature that may be associated with lightning are not expected to be misclassified.

Finally, the average freezing level of the convective pixels was found to be just below 650 hPa (~4 km). Ice presence is a prerequisite for electrical activity, and therefore all strokes should be matched to cloud pixels with altitude above that level. In the case that a stroke is associated to a cloud pixel with altitude lower than 650 hPa (or 4 km), it is considered as artefact, and it is excluded from further analysis.

CTH and CTP are available every 15 min. The nominal time of each SEVIRI scan coincides with the start of the scan. However, central Europe is very close to the end of each 15 min cycle. That introduces a time offset between the scan nominal time slot of the image and the actual time that the imager scans central Europe. To correct this discrepancy, a time shift of 15 min was applied to all CTH and CTP estimations. For example the 15:00 UTC CTH field was treated as representative of 15:15 UTC.

The CTTH algorithm of NWC SAF v2013 allows the computation of CTH in steps of 200 m, and the computation of CTP in steps of 25 hPa. The freezing level in our datasets does not follow that rule, but since the cloud top pressure does, it was decided to examine CCD in steps of 25 hPa too.

Each LINET stroke was associated with the highest cloudy pixel within an area of radius of 0.07 deg. (~7 Km), during the 15 min period around the CTH, CTP or CCD estimation time. This selection is based on the hypothesis that a lightning stroke may travel a certain distance horizontally and therefore it could actually be associated to the next pixel and not the one within which it was detected. A CTH, CTP or CCD value was assigned to every stroke and the total number of strokes was computed for each CTH, CTP and CCD step. Following that, the number of strokes per height (CTH) or pressure (CTP and CCD) step over the analyzed period was summed. The total number of convective pixels per height or pressure step was also computed. As convective pixels we define all those that are not excluded based on the preliminary screenings. Finally, the average Lightning Density (LD) is computed for each height or pressure step as the count of strokes per convective cell, and this average is then reduced to a Lightning Density per hour and degree of latitude and longitude.

Following the PR92 approximation, we seek to create new models of the form $\mathbf{LD} = \mathbf{b_1} \cdot \mathbf{Param}^{\mathbf{b_2}}$, where $\mathbf{b_1}$ is a constant, **Param** refers to each of the three examined parameters (CTH, CTP and CCD), and $\mathbf{b_2}$ is the exponent, which we attempt to define.

To have an unbiased measure of our models' estimation efficiency, we decided to split the available data into two datasets, the “development” and the “control” group. The first one consists of approximately 2/3 of the data, and it is used to actually fit the models. Its members are selected randomly, to ensure the lowest possible bias of the procedure. The rest of the data constitute the control dataset, which is used as an independent dataset reserved for testing the models' performance.

As it will be shown in the next section, the number of convective pixels below and over certain altitudes is very low. Low convective pixels counts may lead to artificially inflated or deflated LD values because LD values are easily influenced by outliers, like a single pixel with extremely high strokes count. To avoid contamination of our datasets with artificial LD values, all data outside the 5% and 95% percentiles of the convective pixels distribution by height were excluded. Since CTH, CTP and CCD are products computed by multi-parametric algorithms, a certain degree of uncertainty is included in their values. At the same time LD is an observational quantity that relies on the accuracy of the detection network. Moreover the altitude uncertainty can also affect the LD values. All these uncertainties should be considered in the modeling process. A methodology able to fulfil that requisite is the Generalized Least Squares technique. A detailed description can be found in York (1966) and Reed (1989, 1992). This method employs the uncertainty of the dependent (in our case the LD) and independent (in our case the CTH, CTP and CDD) parameters of the model. For LD a variance-based estimation of its uncertainty is rather straightforward. The altitude parameters however are computed by the NWC SAF algorithms and there is no way to define a variance value. An acceptable trade-off is to use the minimum step value of these parameters (0.2 km for CTH and 25 hPa for CTP and CCD) as the basis for an uncertainty estimation.

In order to use the Generalized Least Squares methodology, the exponential model $\mathbf{LD} = \mathbf{b_1} \cdot \mathbf{Param_i}^{\mathbf{b_2}}$ is transformed using natural logarithms to $\mathbf{\ln(LD)} = \mathbf{\ln(b_1)} + \mathbf{b_2} \cdot \mathbf{\ln(Param_i)}$.

Then a merit function ($\mathbf{C}$) is computed using the equation:

$$\mathbf{C^2} = \sum_{i=1}^{n} \frac{(\mathbf{\ln(LD_i)} - \mathbf{\ln(b_1)} - \mathbf{b_2 \cdot \ln(Param_i)})}{\mathbf{u^2_{\ln(LD_i)}} + \mathbf{b_2^2 \cdot u^2_{\ln(Param_i)}}} \quad (1)$$

where $\mathbf{u}$ stands for uncertainty. Small values of that function indicate a good fit. $\mathbf{C^2}$ has $\mathbf{n - 2}$ degrees of freedom and follows the chi-square distribution. So, the success of the fit is measured by the probability ($\mathbf{P}$) of the computed $\mathbf{C^2}$ to exceed a certain value. High values of $\mathbf{P}$ suggest a good fit, while small values of $\mathbf{P}$ should be a reason to reject a model. However, this rule of thumb is based on the assumption that the errors follow a normal distribution. In many datasets, the estimation errors do not follow the normal distribution, producing numerous outliers. To compensate for these increased errors, relatively smaller values of $\mathbf{P}$ can be considered as acceptable in the model selection procedure. Finally, the standard errors of the estimated parameters $\mathbf{\ln(b_1)}$ and $\mathbf{b_2}$, are also examined to determine their statistical significance.

After the determination of $\mathbf{b_1}$ and $\mathbf{b_2}$, the skill of each of the models will be assessed with two common and frequently used statistical scores, the Root Mean Square Error (RMSE), and the Mean Biased Error (MBE). These statistics are computed on the control datasets in order to acquire a metric of our model's predicting ability on an independent dataset. They are computed as follows:

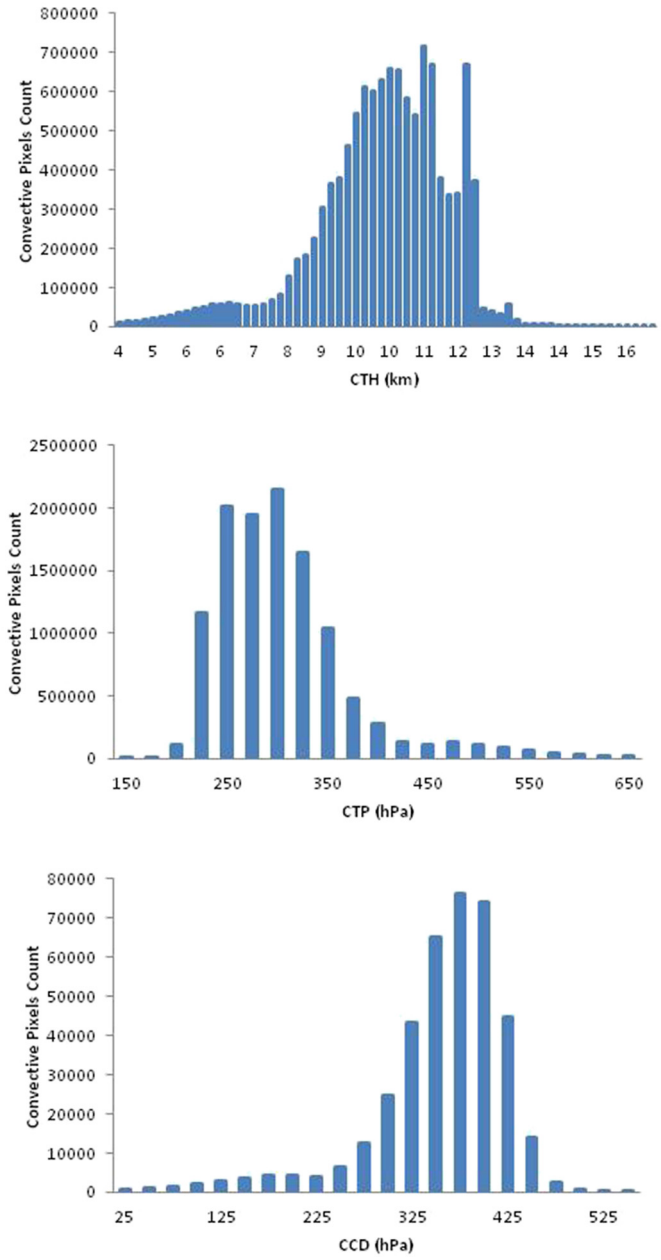

Fig. 3. Convective pixels count per CTH, CTP and CCD step.

$$\mathbf{RMSE} = \sqrt{\frac{\sum_{i=1}^{n} (\mathbf{p_i} - \mathbf{o_i})^2}{\mathbf{n}}} \quad (2)$$

and

$$\mathbf{MBE} = \frac{\sum_{i=1}^{n} (\mathbf{p_i} - \mathbf{o_i})}{\mathbf{n}} \quad (3)$$

with their (%) percentage over the mean value computed by division with the factor $\frac{\sum_{i=1}^{n} o_i}{n}$. The minimization of these statistics indicates that the specific curve produces the smaller differences between the estimated and the observed values of LD. On the contrary, high values suggest that the model does not perform well. However, a fixed value above which the model is considered to be of low predictive ability does not exist, leaving the decision to accept or reject the model to the researcher.

5. Results

Fig. 3 presents the convective pixels counts per CTH, CTP or CCD step over the freezing level. It is obvious that these counts are quite low at both ends of the distribution. As explained earlier, we decided to exclude the upper and lower 5% of data. As a result, the analyzed data range from 8 to 12.4 km for CTH, from 425 to 200 hPa for CTP, and from 300 to 450 hPa for CCD. Regarding the lower limit of the analysis range, is should be mentioned that a similar approach was followed by Ushio et al. (2001), when they analyzed storms of at least 6 km height, while Price and Rind (1992) clearly stated that "clouds with tops below 440 mbar have very little effect on the total lightning frequencies." As for the upper limit, its selection could be further justified through the following considerations: The actual tropopause height, which is a decisive factor for the evolution of convective cloud, although it changes constantly, introducing thus high uncertainty to the overall behaviour of lightning activity around these altitudes, it rarely exceeds 200 hPa (or 12.4 km) in the study area, even during summer. Therefore, it seems pointless to attempt to expand our model applicability to cloud altitudes that are rarely reached over continental Europe. Moreover, the innate uncertainty of the observed data introduces errors that are maximized for extreme altitudes estimations. At this point, according to our previous considerations, it has to be stressed that the proposed models should be considered valid only within the altitude range that was used to formulate them. Outside these limits, significantly erroneous estimations may be produced, especially above the upper altitude limit.

5.1. The CTH model

The coefficients $\mathbf{b_1}$ and $\mathbf{b_2}$, the natural logarithm of $\mathbf{b_2}$ and the standard error values of $\mathbf{ln(b_1)}$ and $\mathbf{b_2}$ are presented in Table 5. The RMSE and MBE, computed as previously mentioned, are also presented. We remind here that the RMSE and the MBE are computed over the control dataset, ensuring thus an independent and unbiased estimation of the efficiency of the model. The visualization of the model curve is illustrated in Fig. 4, along with the CTH-LD points of the "development"and the "control" dataset. The uncertainties of each point on the abscissa and ordinate are also shown as error bars.

The estimated values of $\mathbf{ln(b_1)}$ and $\mathbf{b_2}$ are statistically significant (different than zero) at the 0.95 confidence level, so the developed model is considered as valid. At the same time both RMSE and MBE are acceptable. These two statistics indicate a succesfull model, a fact that is further supported by the visual inspection of Fig. 4, where most of development and control CTH-LD points are situated quite close to the model curve. Only points close to the higher altitudes seem to deviate significantly from the curve. We consider these deviations as a direct result of the approach of the tropopause, which introduce significant deviations from the expected vertical distribution of lightning activity. The possitive value of MBE suggest small overestimation of LD. Overall, following Table 5, the new parameterization is given by the eq. $\mathbf{LD = 1.1 \cdot 10^{-5} \cdot CTH^{7.4}}$ and it is valid inside the height range from 8 to 12.4 km.

Table 5
Coefficients and statistics of the CTH model. RMSE and MBE are in LD units (strokes/(hour·degree^2)).

$ln(b_1)$	$ln(b_1)$ standard error	b_1	b_2	b_2 standard error	RMSE	RMSE (%)	MBE	MBE (%)
−11.4	2.4	$1.1 \cdot 10^{-5}$	7.4	1.0	199.4	39.1	44.1	8.6

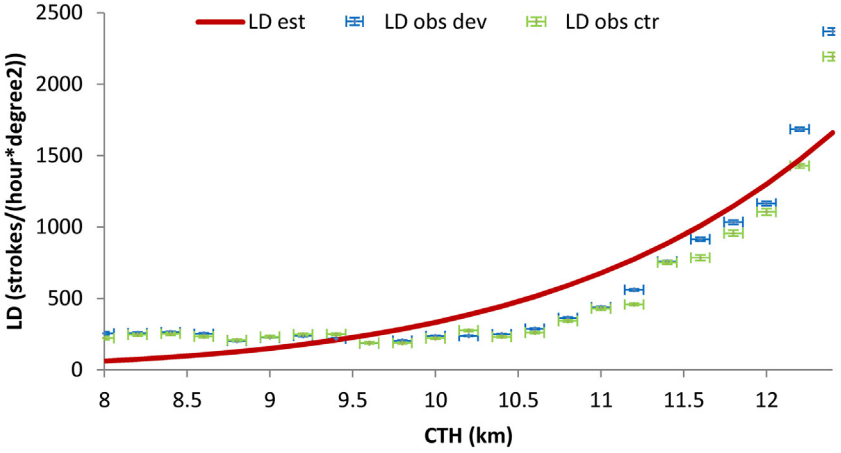

Fig. 4. The CTH model curve (LD Est), overlaid on the CTH-LD points of the development (LD obs dev) and the control (LD obs ctr) datasets.

Table 6
Coefficients and statistics of the CTP model. The RMSE and MBE are in LD units (strokes/(hour·degree^2)).

$ln(b_1)$	$ln(b_1)$ standard error	b_1	b_2	b_2 standard error	RMSE	RMSE (%)	MBE	MBE (%)
30.6	7.0	$1.9{\cdot}10^{13}$	−4.2	1.2	252.6	32.1	105.6	13.4

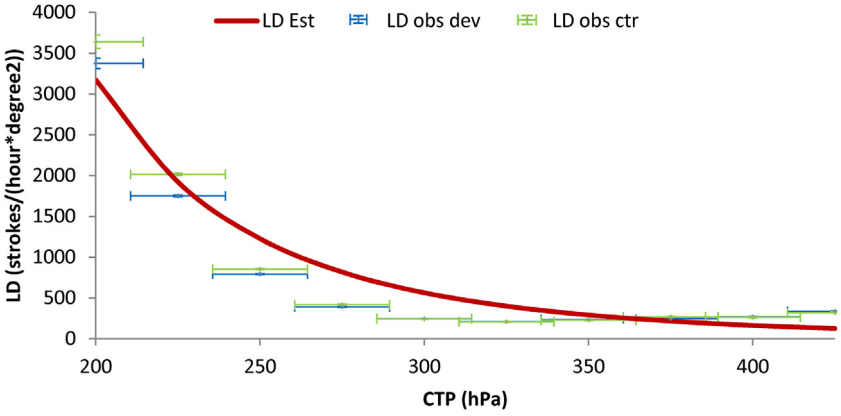

Fig. 5. The CTP model curve (LD Est) overlaid on the CTP-LD points of the development (LD obs dev) and the control (LD obs ctr) datasets.

Table 7
Coefficients and statistics of the CCD model. The RMSE and MBE are in LD units (strokes/(hour·degree^2)).

$ln(b_1)$	$ln(b_1)$ standard error	b_1	b_2	b_2 standard error	RMSE	RMSE (%)	MBE	MBE (%)
−19.7	3.7	$2.8{\cdot}10^{-9}$	4.4	0.6	247.4	35.1	1.7	0.2

5.2. The CTP model

Coefficient $\mathbf{b_2}$ of the CTP model ($\mathbf{LD = b_1 \cdot CTP^{b_2}}$) is expected to be negative because barometric pressure decreases as the altitude increases. The coefficients and error statistics of the model are presented in Table 6 while Fig. 5 shows the model curve and the CTP-LD points of the "development"and "control" datasets.

Just like in the case of the CTH-LD model, the $\mathbf{ln(b_1)}$ and $\mathbf{b_2}$ are statistically significant at the 0.95 confidence level, while RMSE and MBE are also acceptable. The possitive value of MBE indicates an overestimation of LD. The visual inspection of Fig. 5, suggest a good fit since most of the development and control CTH-LD points are very near the model curve. Overall, the prososed parameterization, $\mathbf{LD = 1.9 \cdot 10^{13} \cdot CTP^{-4.2}}$, is considered valid inside the pressure levels that range from 425 to 200 hPa.

5.3. The CCD model

Table 7 presents the coefficients and statistics of the $\mathbf{LD = b_1 \cdot CCD^{b_2}}$ model, while Fig. 6, depicts the model curve and the CCD-LD points of the "development"and "control" dataset. The values of $\mathbf{ln(b_1)}$ and $\mathbf{b_2}$ are statistically significant at the 0.95 confidence level and RMSE and MBE have acceptable values. The examination of the differences at each point of the control dataset indicates that the relatively increased RMSE values are mostly atributed to the deviations at 450 hPa. In fact the 450 hPa control LD value seems to deviate significantly from the pattern of the development dataset, and also from the patterns of the control datasets of the previous 2 models. This could be the result of the sparsier sampling of the CCD parameter, which constitutes of 4 values per day, in contrast to the 96 values per day for CTH and CTP. MBE has a negligible positive value. Concluding, the model $\mathbf{LD = 2.8 \cdot 10^{-9} \cdot CCD^{4.4}}$ is considered valid in the CCD range from 300

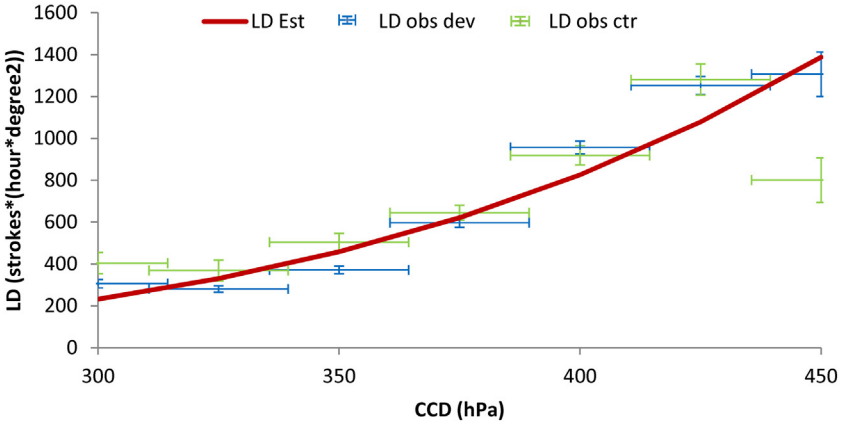

Fig. 6. The CCD model curve (LD Est) overlaid on the CCD-LD points of the development (LD obs dev) and the control (LD obs ctr) datasets.

to 450 hPa.

6. Discussion and conclusions

A reassessment of the PR92 parameterization between cloud top height and lightning density was attempted in the present work. Besides the cloud top height (CTH), two more parameters, the cloud top pressure (CTP) and the cold cloud depth (CCD) were examined, aiming to propose additional parameterization schemes. Our dataset was split in two parts, the "development" dataset and the "control" dataset. The first one was used to develop the new parameterizations and the second one to cross-validate them.

The lightning data used for the analysis were provided from LINET network and they cover the summer period of 2016. Each lightning stroke was associated to an eligible convective cloud pixel and thus a Cloud Top Height (CTH), Cloud Top Pressure (CTP), and Cold Cloud Depth (CCD) value was assigned to it. The eligible convective pixels were selected among all cloudy pixels after a screening based on their cloud type (CT, NWC SAF product), convective nature (CRR, NWC SAF product) and temperature (comparison with ERA-Interim derived average freezing level).

For each of the eligible convective pixels a Lightning Density (LD) value was computed and then the average LD for each CTH, CTP and CCD step was calculated. Since convective pixels counts in the upper and lower parts of the distribution are very small, we decided to exclude the lower and upper 5% of the data in order to avoid including artificially inflated or deflated LD values in our analysis. After the exclusion of that data, the valid altitude ranges were 8–12.4 km for CTH, 425–200 hPa for CTP and 300–450 hPa for CCD. As a consequence the new parameterizations are considered valid only within these specific altitude ranges.

To further reduce the possibility of biased results by the variability of the observational data, the exponential models were transformed to linear and a Generalized Linear Regression methodology was applied.

It was shown that the formulation of a relationship between the cloud top altitude and the lightning activity is feasible for all 3 examined parameters (CTH, CTP and CCD). The derived formulas are the following:

$$LD = 1.1 \cdot 10^{-5} \cdot CTH^{7.4} \quad (4)$$

$$LD = 1.9 \cdot 10^{13} \cdot CTP^{-4.2} \quad (5)$$

$$LD = 2.8 \cdot 10^{-9} \cdot CCD^{4.4} \quad (6)$$

The cross-validation of these models against the control dataset yield acceptable RMSE and MBE values, suggesting a successful fit. A small overestimation of the LD is evident, ranging from 0.2% to 13.4%.

Since these parameterizations were formulated using data over continental Europe during summertime, these three models could be considered valid for mid-latitude continental regions during the warm period of the year.

In our analysis we did not consider the time evolution of selected storms. In fact, our models were based on the analysis of all recorded strokes over a three month period, without any effort to distinguish different storms or different stages of storm development. For this reason, it is suggested to avoid the proposed relationships for the computation of instantaneous LD values. Instead, the proposed relationships could be used in numerical modeling for deriving LD values over larger timescales (e.g. hourly values of LD), where the stroke counts are rather free of small-scale temporal variations. Climate projections could also use these relationships in order to estimate future trends in lightning.

The exponent of CTH of our model is equal to 7.4, a value that differs from the one proposed by the PR92 parameterization, and supports a more rapid increase of activity with the increase of cloud top height. Reservations on the applicability of the PR92 parameterization have been introduced by many researchers (Michalon et al. (1999), Ushio et al. (2001), Boccippio (2002), Barthe et al. (2010)), as discussed in the introduction section. According to our findings, these reservations seem to be justified. However, the PR92 parameterization may still be applicable on a global scale, throughout the year. We remind that our analysis was restricted over continental Europe, during summer time. Equatorial or subtropical regions, or even other mid-latitude regions during different periods of the year, may present different behaviour, regarding the cloud top altitude and lightning density relationship, which could be closer to the PR92 parameterization.

Finally, it is our belief that the proposed parameterizations could be utilized within numerical model simulations to produce quantitative estimations of the amount of strokes over convective areas. The authors believe that the input of modelers who may experiment with the proposed parameterizations are really valuable and welcome them.

Acknowledgements

The authors would like to thank EUMETSAT for the provision of the satellite imagery and of the NWC SAF software.

References

Ashley, W.S., Gilson, C.W., 2009. A reassessment of U.S. lightning mortality. B. Am. Meteorol. Soc. 90, 1501–1518.

Barthe, Chr, Deierling, W., Barth, M.C., 2010. Estimation of total lightning from various storm parameters: a cloud resolving study. J. Geophys. Res. 115, D24202.

Berrisford, P., Dee, D.P., Poli, P., Brugge, R., Fielding, K., Fuentes, M., Kållberg, P.W., Kobayashi, S., Uppala, S., Simmons, A., 2011. The ERA-interim archive. ERA Rep. Ser. 1, 1–16.

Betz, H.D., Schmidt, K., Laroche, P., Blanchet, B., Oettinger, W.P., Defer, E., Dziewit, Z., Konarski, J., 2009a. LINET-An international lightning detection network in Europe. Atmos. Res. 91, 564–573.

Betz, H.D., Schmidt, K., Oettinger, W.P., 2009b. LINET – An International VLF/LF lightning detection network in Europe. In: Betz, H.D., Schumann, U., Laroche, P. (Eds.), Lightning: Principles, Instruments and Applications. Springer, Dordrecht.
Boccippio, D.J., 2002. Lightning Scaling Relations Revisited. J. Atmos. Sci. 59, 1086–1104.
Cardoso, I., Pinto Jr., O., Pinto, I.R.C.A., Holle, R., 2014. Lightning casualty demographics in Brazil and their implications for safety rules. Atmos. Res. 135–136, 374–379.
Chang, J.I., Lin, C.C., 2006. A study of storage tank accidents. J. Loss Prevent. Proc. 19 (1), 51–59.
Cherington, M., Mathys, K., 1995. Deaths and injuries as a result of lightning strikes to aircraft. Aviat. Space Environ. Md. 66 (7), 687–689.
Coates, L., Blong, R., Siciliano, F., 1993. Lightning fatalities in Australia, 1824–1991. Nat. Hazards 8 (3), 217–233.
Dee, D.P., Uppala, S.M., Simmons, A.J., Berrisford, P., Poli, P., Kobayashi, S., Andrae, U., Balmaseda, M.A., Balsamo, G., Bauer, P., Bechtold, P., Beljaars, A.C.M., Van de Berg, L., Bidlot, J., Bormann, N., Delsol, C., Dragani, R., Fuentes, M., Geer, A.J., Haimberger, L., Healy, S.B., Hersbach, H., Hólm, E.V., Isaksen, L., Kållberg, P., Köhler, M., Matricardi, M., McNally, A.P., Monge-Sanzf, B.M., Morcrette, J.J., Park, B.K., Peubey, C., De Rosnay, P., Tavolato, C., Thépaut, J.N., Vitart, F., 2011. The ERA-Interim reanalysis: configuration and performance of the data assimilation system. Q. J. R. Meteo. Soc. 137, 553–597.
Derrien, M., Le Gléau, H., 2013a. Algorithm Theoretical Basis Document for "Cloud Products" (CMa-PGE01 v3.2, CT-PGE02 v2.2 & CTTH-PGE03 v2.2). EUMETSAT.
Derrien, M., Le Gléau, H., 2013b. Product User Manual for "Cloud Products".(CMa-PGE01 v3.2, CT-PGE02 v2.2 & CTTH-PGE03 v2.2). EUMETSAT.
Derrien, M., Le Gléau, H., 2013c. Validation Report for "Cloud Products" (CMa-PGE01 v3.2, CT-PGE02 v2.2 & CTTH-PGE03 v2.2). EUMETSAT.
Dudhia, J., 1989. Numerical study of convection observed during the winter monsoon Experiment using a mesoscale two-dimensional model. J. Atmos. Sci. 46, 3077–3107.
Elsom, D.M., 2001. Deaths and Injuries Caused by Lightning in the United Kingdom: analyses of two databases. Atmos. Res. 56, 325–334.
EUMETSAT Nowcasting Consortium, 2013. Software User Manual for the SAFNWC/MSG Application (SAF-NWC-CDOP2-INM-MGT-SUM_v7.0). EUMETSAT.
Flannigan, M.D., Wotton, B.M., 1991. Lightning-ignited forest fires in northwestern Ontario. Can. J. For. Res. 21, 277–287.
Giannaros, T.M., Kotroni, V., Lagouvardos, K., 2015. Predicting lightning activity in Greece with the Weather Research and Forecasting (WRF) model. Atmos. Res. 156, 1–13.
Giannaros, T.M., Kotroni, V., Lagouvardos, K., 2016. WRF-LTNGDA: a lightning data assimilation technique implemented in the WRF model for improving precipitation forecasts. Environ. Model. Softw. 76, 54–68.
Gijben, M., Dyson, L.I., Loots, M.T., 2017. A statistical scheme to forecast the daily lightning threat over southern Africa using the Unified Model. Atmos. Res. 194, 78–88.
Janjic, Z.I., 1994. The step-mountain Eta coordinate model: further developments of the convection, viscous sublayer and turbulence closure schemes. Mon. Weather Rev. 122, 927–945.
Janjic, Z.I., 1996. The surface layer in the NCEP Eta model. In: 11th Conference on Numerical Weather Prediction, Norfolk, VA, USA.
Janjic, Z.I., 2002. Nonsingular Implementation of the Mellor-Yamada Level 2.5 Scheme in the NCEP Meso Model. NCEP Office Note, No 437.
Kain, J.S., 2004. The Kain–Fritsch convective parameterization: an update. J. Appl. Meteorol. 43, 170–181.
Karagiannidis, A., Lagouvardos, K., Kotroni, V., 2016. The use of lightning data and Meteosat Infrared imagery for the nowcasting of lightning activity. Atmos. Res. 168, 57–69.
Kohn, M., Galanti, E., Price, C., Lagouvardos, K., Kotroni, V., 2011. Nowcasting thunderstorms in the Mediterranean region using lightning data. Atmos. Res. 100, 489–502.
Krausmann, E., Renni, E., Campedel, M., Cozzani, V., 2011. Industrial accidents triggered by earthquakes, floods and lightning: lessons learned from a database analysis. Nat. Hazards 59, 285–300.
Liu, W., Wang, S., Zhou, Y., Wang, L., Zhang, M., 2010. Lightning-caused forest fires risk assessment based on historical fires events in Daxingan Mountains of China. Disaster Adv. 3 (4), 143–147.
Michalon, N., Nassif, A., Saouri, T., Royer, J.F., Pontikis, C.A., 1999. Contribution to the climatological study of lightning. Geophys. Res. Lett. 26 (20), 3097–3100.
Mlawer, E.J., Taubman, S.J., Brown, P.D., Iacono, M.J., Clough, S.A., 1997. Radiative transfer for inhomogeneous atmospheres: RRTM, a validated correlated-k model for the longwave. J. Geophys. Res. 102, 166663–166682.
Molinié, J., Pontikis, C.A., 1995. A climatological study of tropical Thunderstorm clouds and lightning frequencies on the French Guyana coast. Geophys. Res. Lett. 22 (9), 1085–1088.
Molinié, J., Pontikis, C.A., 1996. Reply [to "Comment on 'A climatological study of tropical Thunderstorm clouds and lightning frequencies on the French Guyana coast.' by Molinié, J., and Pontikis C.A."]. Geophys. Res. Lett. 23 (13), 1703–1704.
Papagiannaki, K., Lagouvardos, K., Kotroni, V., 2013. A database of high-impact weather events in Greece: a descriptive impact analysis for the period 2001–2011. Nat. Hazard. Earth Syst. 13, 727–736.
Peterson, D., Wang, J., Ichoku, C., Remer, L.A., 2010. Effects of lightning and other meteorological factors on fire activity in the north American boreal forest: implications for fire weather forecasting. Atmos. Chem. Phys. 10 (14), 6873–6888.
Price, C., Rind, D., 1992. A simple lightning parameterization for calculating global lightning distributions. J. Geoph. Res. 97 (D9), 9919–9933.
Pytharoulis, I., Kotsopoulos, S., Tegoulias, I., Kartsios, S., Bampzelis, D., Karacostas, T., 2016. Numerical modeling of an intense precipitation event and its associated lightning activity over northern Greece. Atmos. Res. 169, 523–538.
Reed, B.C., 1989. Linear least-squares fits with errors in both coordinates. Am. J. Phys. 57, 642–646.
Reed, B.C., 1992. Linear least-squares fits with errors in both coordinates. II: comments on parameter variances. Am. J. Phys. 60, 59–62.
Renni, E., Kraussmann, E., Cozzani, V., 2010. Industrial accidents triggered by lightning. J. Hazard.Mater. 184, 42–48.
Rodríguez, A., Marcos, C., Manso, M., 2013a. Algorithm Theoretical Basis Document for "Convective Rainfall Rate" (CRR-PGE05 v4.0). EUMETSAT.
Rodríguez, A., Marcos, C., Manso, M., 2013b. Product User Manual for "Convective Rainfall Rate" (CRR-PGE05 v4.0). EUMETSAT.
Rodríguez, A., Marcos, C., Manso, M., 2013c. Validation Report for "Convective Rainfall Rate" (CRR-PGE05 v4.0). EUMETSAT.
Rorig, M.L., Ferguson, S.A., 1999. Characteristics of lightning and wildland fire ignition in the Pacific Northwest. J. Appl. Meteorol. 38, 1565–1575.
Skamarock, W.C., Klemp, J.B., Dudhia, J., Gill, D.O., Barker, D.M., Duda, M.G., Huang, X.Y., Wang, W., Powers, J.G., 2008. A Description of the Advanced Research WRF Version 3. NCAR Technical Note: NCAR/TN-475 + STR. Mesoscale and Microscale Meteorology Division, National Centre for Atmospheric Research, Boulder, CO, USA.
Tewari, M., Chen, F., Wang, W., Dudhia, J., LeMone, M.A., Mitchell, K., Ek, M., Gayno, G., Wegiel, J., Cuenca, R.H., 2004. Implementation and verification of the Unified NOAH land surface model in the WRF model. In: 20th Conference on Weather Analysis and Forecasting/16th Conference on Numerical Weather Prediction, pp. 1115.
Thompson, G., Field, P.R., Rasmussen, R.M., Hall, W.D., 2008. Explicit forecasts of winter precipitation using an improved bulk microphysics scheme-Part II: implementation of a new snow parameterization. Mon. Weather Rev. 136, 5095–5115.
Ushio, T., Heckman, S.T., Boccippio, D.J., Christian, H.J., Kawasaki, Z.I., 2001. A survey of thunderstorm flash rates compared to cloud top height using TRMM satellite data. J. Geophys. Res. 106, 24089–24095.
Wong, J., Barth, M.C., Noonem, D., 2013. Evaluating a lightning parameterization based on cloud-top height for mesoscale numerical model simulations. Geosci. Model Dev. 6, 429–443.
Yair, Y., Lynn, B., Price, C., Kotroni, V., Lagouvardos, K., Morin, E., Mugnai, A., Llasat, M.D.C., 2010. Predicting the potential for lightning activity in Mediterranean storms based on the Weather Research and forecasting (WRF) model dynamic and microphysical field. J. Geophys. Res. Atmos. 115, D04.
York, D., 1966. Least-squares fitting of a straight line. Can. J. Phys. 44, 1079–1086.
Yoshida, S., Morimoto, T., Ushio, T., Kawasaki, Z.I., 2009. A fifth-power relationship for lightning activity from Tropical Rainfall Measuring Mission satellite observations. J. Geophys. Res. Atmos. 114, D09.
Zepka, G.S., Pinto Jr., O., Saraiva, A.C.V., 2014. Lightning forecasting is southeastern Brazil using the WRF model. Atmos. Res. 135–136, 344–362.